Theor Chem Acc (2002) 107:351–356
DOI 10.1007/s00214-002-0339-9

Theoretical
Chemistry Accounts

Regular article

Ab initio structure and vibrational frequencies of lithium aromatic sulfonyl imide salts

S. P. Gejji, P. R. Agrawal, N. R. Dhumal

Department of Chemistry, University of Pune, Pune 411 007, India

Received: 20 February 2002 / Accepted: 25 March 2002 / Published online: 3 June 2002

Abstract. The structure and vibrational frequencies of an aromatic lithium sulfonyl imide, i.e., lithium bis(4-nitrophenylsulfonyl)imide (LiNPSI) has been studied using self-consistent ab initio Hartree–Fock and hybrid density functional methods. These calculations engender two linkage isomers, which correspond to the local minima on the potential-energy surface. In the lowest-energy isomer, the ligand binds to the metal ion through two oxygens, one from each of the different SO_2 groups on the central nitrogen and forms a six-membered ring. Another LiNPSI isomer, wherein the anion coordinates through oxygen and nitrogen atoms and which is 55.9 kJmol^{-1} higher in energy, has also been obtained. The S–N–S bond angle in the free anion as well as in the LiNPSI complex turns out to be nearly 121°. A comparison of the vibrational spectra of the free NPSI anion and that of the LiNPSI complex reveals that the SO_2 stretching vibrations at 1,239 and 1,205 cm^{-1} can be used to differentiate between the two linkage isomers of the complex. The stronger complexation ability of the NPSI anion, compared to that for $(CF_3SO_2)_2N^-$ has been explained in terms of the charge density within the molecular electrostatic potential isosurface encompassing both SO_2 groups of the anion.

Key words: Molecular electrostatic potential – Hartree–Fock – Hybrid density functional methods

1 Introduction

Solid polymer electrolytes (SPE) composed of alkali-metal salts, for example, lithium salts of trifluromethanesulphonate (triflates) $CF_3SO_3^-$ [1] or bis(trifluromethanesulphone)imide (TFSI) anion $(CF_3SO_2)N^-$ [2, 3], dissolved in poly(ethylene oxide) (PEO) or its oligomers are of great interest for being the vital components of high-energy density batteries and electrochromic devices [4]. The significant ionic conductivity exhibited by these SPE depends on different factors, such as polymer segmental motion, cation–polymer interaction, and ionic association. Amongst these, the ionic association comprising of ion pairs and triplets or higher aggregates can be monitored by IR or Raman spectroscopy experiments [5, 6, 7]. In recent years, theoretical calculations based on ab initio molecular orbital (MO) methods or hybrid density functional theory have been employed to analyze the structural and spectral consequences of the ion pairing [4, 8]. These investigations provide insight into the binding patterns of these molecular systems. Electrostatic models have been used widely for predicting the structures and binding in the van der Waals or hydrogen-bonded or ion-pair complexes [9, 10, 11, 12, 13, 14, 15]. An alternative to the expensive lithium salts of fluoride-containing superacids such as triflate or TFSI can be devised through the synthesis of new plasticizers, for example, aromatic lithium sulfonyl imides. One such salt developed recently is the lithium salt of the bis(4-nitrophenylsulfonyl)imide (NPSI) anion, wherein the electron-withdrawing NO_2 substituents at both phenyl groups are responsible for the delocalization of negative charge over the larger space and thereby for generating a higher charge carrier concentration [16, 17] in the SPE. The flexibility of the S–N–S framework is also important in governing the mobility of the anion. We, therefore, derive the electronic structure, the charge distribution, and the vibrational frequencies of the NPSI anion by employing ab initio quantum chemical and hybrid density functional methods and investigate the nature of the coordination of $NPSI^-$ to the lithium cation using the molecular electrostatic potential (MESP) [5] topography as a tool. This approach has proven useful in the case of triflate and TFSI anions reported in the literature [18]. The computational method is outlined in the following section.

2 Computational method

Ab initio Hartree–Fock (HF) self-consistent MO calculations were performed for the free anion using the GAUSSIAN 94 program

Correspondence to: S. P. Gejji

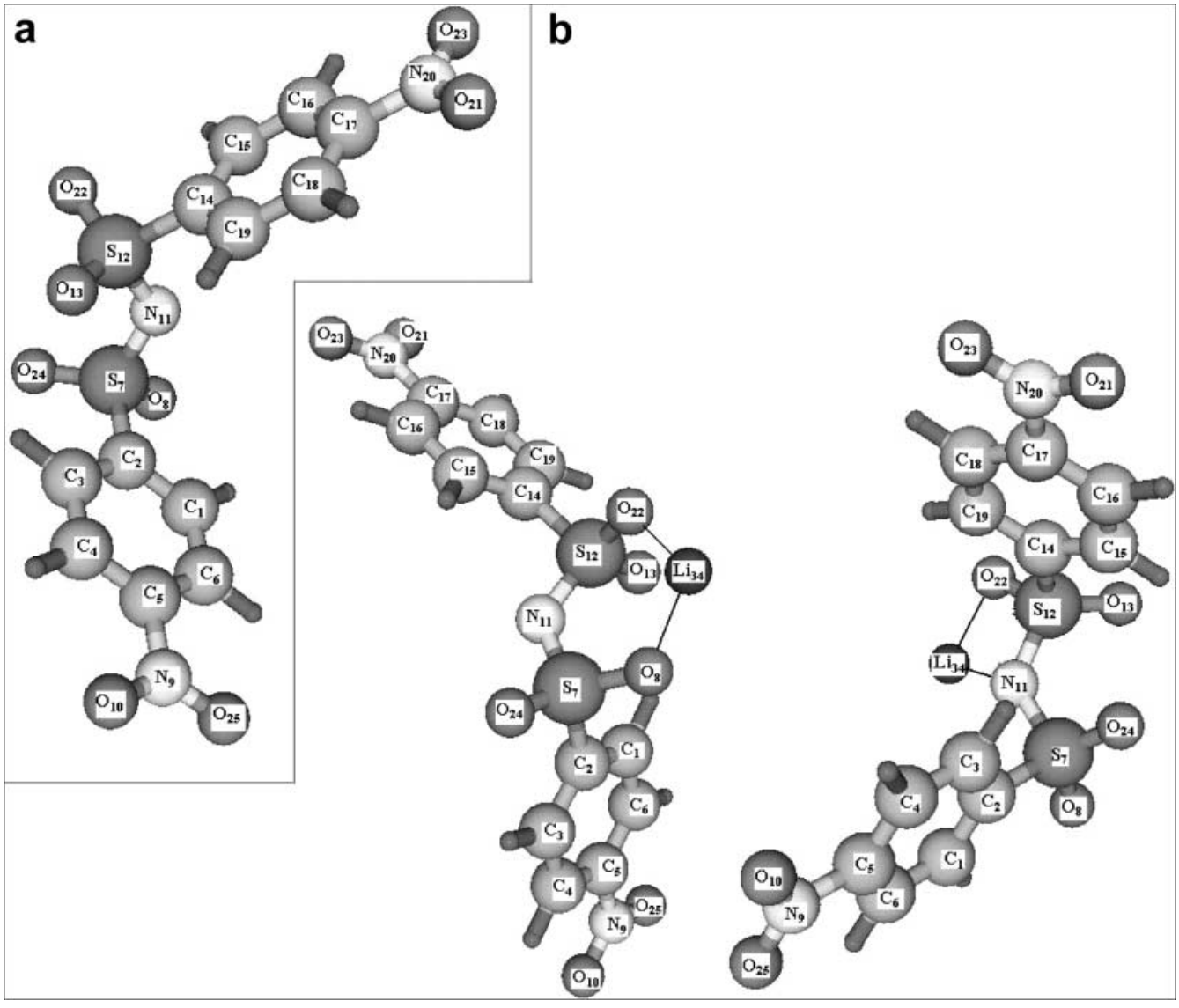

Fig. 1. a Optimized geometries of the bis(4-nitrophenylsulfonyl)imide (*NPSI*) anion and **b** the LiNPSI isomers A and B

[19] with the internally stored 6-31G(d, p) basis. The MESP, $V(\mathbf{r})$, at a point $\mathbf{r}$ due to a molecular system with nuclear charges $\{\boldsymbol{Z}_\mathbf{A}\}$ located at $\{\mathbf{R}_A\}$ and electron density $\rho(\mathbf{r})$ is defined by

$$V(\mathbf{r}) = \sum_{A=1}^{N} \frac{Z_A}{|\mathbf{r} - \mathbf{R}_A|} - \int \frac{\rho(\mathbf{r}')\mathrm{d}^3\mathbf{r}'}{|\mathbf{r} - \mathbf{r}'|} \quad , \tag{1}$$

with N being the total number of nuclei in the molecule. The first term in Eq. (1) refers to the bare nuclear potential and the second term to the electronic contribution. The topography of the MESP is mapped by examining the eigenvalues of the Hessian matrix at the point where the gradient $V(\mathbf{r})$ vanishes. The critical points (CPs) derived from the computed MESP were visualized by using the package UNIVIS-2000 [20]. These CPs can be characterized in terms of an ordered pair (rank and signature) and further grouped into three sets, viz., (3, −3), (3, −1), (3, 1) and (3, 3). The (3, 3) correspond to the set of MESP minima and the remaining ones represent the saddle points. Thus, the MESP minima were employed as the potential cation-binding sites in the cation–anion complex.

The lithium cation was placed in the vicinity of the MESP minima of the anion and the resulting Li^+NPSI^- geometries were subsequently subjected to the HF optimization. The geometries thus obtained were further optimized using hybrid density functional theory employing Becke's [21] three-parameter exchange with Lee, Yang, and Parr's correlation functional [22] (B3LYP) method. All stationary point geometries were characterized by examining the number of imaginary frequencies and the eigenvalues of the Hessian matrix. Normal vibrations from the B3LYP theory were assigned by visualizing the displacement of the atoms around their equilibrium positions using the program UNIVIS-2000 [20].

3 Results and discussion

In order to investigate the LiNPSI complex formation, the presence of charge carriers being one of the key factors in governing the ionic conductivity of SPE, we studied the MESP topography of the NPSI anion. The MESP topography of the anion shows in all 56 negative CPs. For the NPSI anion the numbers of (3, 3), (3, 1), and (3, −1) CPs turn out to be 14, 29, and 13, respectively. O_8 and O_{13} atoms in the anion possess

only a single (3, 3) CP, whereas the rest of the oxygen atoms show a doublet of CPs. The MESP minima, below -450 kJmol^{-1}, are nearly 1.25 Å from the respective oxygens. The Li^+ was placed in the vicinity of these minima and six different initial geometries for the LiNPSI complex were generated. On subsequent optimization, the HF method finally converged to two linkage isomers, A and B, which are displayed along with the atom labels in Fig. 1. In the lowest-energy structure of the LiNPSI complex, the O_{22} and O_8 atoms of the different SO_2 groups coordinate with the cation as has been found in the case of the LiTFSI complex. In isomer B the coordination occurs through N_{11} and O_{13} atoms. The B3LYP theory predicts isomer A to be stabilized by 55.9 kJmol^{-1} more than isomer B, which may partly be attributed to the formation of a six-membered chelate.

The B3LYP optimized geometrical parameters of the $NPSI^-$ and the LiNPSI isomers are presented in Table 1. Selected geometrical parameters for the $(CF_3SO_2)_2N^-$ are also given. As may be noticed readily, the $S_{12}N_{11}$ and S_7N_{11} bonds in the NPSI anion are longer by 0.007 and 0.008 Å, respectively, compared to the corresponding bonds in the TFSI anion. A closure of the S–N–S bond angle (by nearly 2°) was noticed for $NPSI^-$. Comparison of $NPSI^-$ and LiNPSI isomers A and B shows that the coordination results in the elongation (0.04 Å) of the S_7O_8 and $S_{12}O_{22}$ bonds. The bond angles are less sensitive to the coordination and generally show a largest deviation of 3°.

As may readily be noticed, the S–N bonds of the LiNPSI complex in isomer B are longer ($S_{12}N_{11}$ 0.023 Å, S_7N_{11} 0.058 Å) compared to the corresponding bonds in isomer A, because only in the former complex the nitrogen of the ligand binds to the cation. The bond angles in the two isomers compare well except for the N–S–O angles, which show a largest deviation of 10° (Table 1). Bidentate coordination of oxygens of the $NPSI^-$ in isomer A results in a change of orientation of the nitrophenyl ring, which is pushed below the $C_{14}S_{12}N_{11}$ plane of the anion by 30° (Fig. 1). In isomer B this nitrophenyl ring orients itself in the opposite direction to the $C_{14}S_{12}N_{11}$ plane when compared with that of the free anion.

B3LYP vibrational frequencies, scaled by 0.9613, in the region 470–1,700 cm^{-1} for $NPSI^-$ and the LiNPSI

Table 1. B3LYP optimized geometrical parameters (bond lengths in angstroms and bond angles in degrees) of thebis(trifluromethanesulphone)imide anion (*TFSI*$^-$), bis(4–nitrophenylsulfonyl)imide anion (*NPSI*$^-$), and LiNPSI isomers

	TFSI	NPSI	Li^+NPSI^- (A)	Li^+NPSI^- (B)
$r(S_7C_2)$	1.873	1.813	1.794	1.808
$r(S_7O_8)$	1.469	1.475	1.517	1.465
$r(N_9C_5)$		1.466	1.477	1.476
$r(N_9O_{10})$		1.234	1.229	1.230
$r(S_7N_{11})$	1.620	1.628	1.615	1.673
$r(S_{12}N_{11})$	1.620	1.627	1.621	1.644
$r(S_{12}O_{13})$	1.468	1.472	1.461	1.514
$r(S_{12}C_{14})$	1.873	1.819	1.802	1.801
$r(N_{20}C_{17})$		1.465	1.476	1.477
$r(N_{20}O_{21})$		1.234	1.229	1.229
$r(S_{12}O_{22})$	1.469	1.474	1.514	1.460
$r(N_{20}O_{23})$		1.234	1.229	1.229
$r(S_7O_{24})$	1.468	1.483	1.474	1.469
$r(N_9O_{25})$		1.233	1.230	1.230
$r(O_{22}Li_{34})$			1.818	1.878
$a(C_2S_7O_8)$	104.3	105.2	106.8	106.5
$a(C_4C_5N_9)$		118.9	118.7	118.7
$a(C_5C_9O_{10})$		118.0	117.5	117.5
$a(C_2S_7N_{11})$	102.8	97.1	100.1	100.2
$a(S_7N_{11}S_{12})$	123.9	121.6	122.8	122.6
$a(N_{11}S_{12}O_{13})$	108.0	107.0	109.5	98.5
$a(N_{11}S_{12}C_{14})$	102.8	104.7	106.9	109.5
$a(N_{11}S_7O_{24})$	108.0	114.8	116.1	110.6
$a(C_{16}C_{17}N_{20})$		119.0	118.7	118.8
$a(C_{17}N_{20}O_{21})$		118.1	117.5	117.5
$a(N_{11}S_7O_{24})$		114.8	116.1	110.6
$a(C_5N_9O_{25})$		118.0	117.5	117.5
$a(C_{14}S_{12}O_{22})$	117.0	105.1	104.8	107.5
$a(C_{17}N_{20}O_{23})$		118.1	117.5	117.5
$a(S_{12}O_{22}Li_{34})$			122.8	94.4
$d(O_8S_7C_2C_3)$		114.4	104.1	166.1
$d(N_{11}S_7C_2C_3)$		−128.3	−139.5	−80.2
$d(S_{12}N_{11}S_7C_2)$	90.9	161.3	−168.7	136.4
$d(O_{13}S_{12}N_{11}S_7)$	−160.1	160.5	146.5	168.2
$d(C_{14}S_{12}N_{11}S_7)$	90.9	−88.6	−97.4	−81.3
$d(C_{15}C_{14}S_{12}N_{11})$		82.0	51.5	87.6
$d(O_{22}S_{12}C_{14}C_{15})$		−39.2	−67.3	−39.8
$d(O_{24}S_7N_{11}S_{12})$	90.9	50.1	74.9	23.2
$d(C_{14}S_{12}O_{22}Li_{34})$			139.7	−123.4

Table 2. Selected B3LYP vibrational frequencies (cm^{-1}) of the $TFSI^-$, $NPSI^-$, and LiNPSI isomers

Assignment	TFSI	NPSI	Li^+NPSI^- (A)	Li^+NPSI^- (B)
NO_2 stretch + CC stretch		1,597	1,610	1,609
		1,594	1,609	1,608
CC stretch		1,574	1,577	1,576
		1,571	1,577	1,575
CC stretch + NO_2 stretch		1,542	1,561	1,559
		1,540	1,559	1,559
CCH rock		1,456	1,464	1,457
		1,456	1,458	1,457
NO_2 stretch + CN stretch		1,340	1,347	1,346
		1,336	1,345	1,344
CC stretch		1,382	1,384	1,382
		1,381	1,383	1,381
CC stretch + OCS bend		1,324	1,321	1,319
		1,324	1,319	1,317
CCH rock		1,269	1,277	1,272
		1,265	1,267	1,268
SO_2 stretch	1,273	1,239	1,217	1,257
	1,250	1,205	1,167	1,232
CCH scissor		1,155	1,162	1,156
		1,152	1,154	1,151
CS stretch + SO_2 stretch		1,094		1,092
CCH scissor			1,091	
			1,084	1,086
CCC bend + CN stretch		1,084	1,083	1,083
		1,084	1,082	1,081
		1,080		1,081
SO stretch + SN stretch	1,069			
CS stretch + CCC bend			1,069	1,068
CS stretch		1,049		1,043
SN stretch + CCC bend		1,032	1,023	
CCC bend		995	1,001	996
		993	989	991
			982	976
CCH twist			963	
CCH twist + SN stretch	960	960	961	961
CCH twist		958	961	958
		947	956	956
CCH twist		946	956	954
				926
CCH wag		843	851	847
		837	848	844
CCC bend + NO_2 bend		833	834	833
		832	832	832
CCH wag			829	824
		816	822	822
		815		
CCC bend + SN stretch	738		744	750
NO bond oscillation		733	729	726
		730	728	724
CS stretch	722			
CCC bend		712	716	719
SNS bend	688	682	685	703
NO bond oscillation		672	671	665
NCS bend		660		666
OLi stretch			637	635
SNS bend		624		
OLi stretch			626	
CCC bend		613	612	612
		611	610	611
NLi stretch				567
SO_2 bend + NCS bend	579	566		
OLi stretch				558
OLiO bend			541	
CNO bend		516	518	517
			517	515
NCC bend		509		
CCC bend		525		
OSN bend		522		
OLiO bend			479	506

complex are reported in Table 2. The frequencies of some of the normal vibrations in $TFSI^-$ are also given. For free $TFSI^-$, two intense SO_2 stretching vibrations at 1,273 and 1,250 cm^{-1} were observed. In isomer A, the two SO_2 stretching vibrations shift to a lower value, viz., 1,217 and 1,167 cm^{-1}, owing to the bidentate coordination through two oxygens, whereas in isomer B these vibrations shift by about 17 cm^{-1} to higher values. Thus, the direction of the frequency shift of these vibrations may enable one to distinguish the LiNPSI isomers A and B. The S–N stretching of $TFSI^-$ assigned to the 1,069 and 960 cm^{-1} vibrations corresponds to intense 1,032 and 960 cm^{-1} vibrations of free $NPSI^-$. This is in accordance with the S–N bond lengths in this anion. Table 2 shows that the coordination of $NPSI^-$ to the metal results in the appearance of new bands at 1,069 and about 637 cm^{-1} in both the LiNPSI structures. A very intense 1,023 cm^{-1} vibration attributable to S–N stretching coupled with different bendings was obtained only for the lowest-energy isomer A. For isomer B, relatively intense 926 and 750 cm^{-1} vibrations have been predicted. The former of these vibrations, however, can neither be correlated to any of the normal vibrations in isomer A nor to any of those of the free anion. Further, the relatively intense 626 and 558 cm^{-1} vibrations of isomers A and B, respectively, were assigned to the O–Li stretchings.

The complexation of $NPSI^-$ and $TFSI^-$ with Li^+ was compared by visualizing the MESP (−370.2 $kJmol^{-1}$) isosurface encompassing the SO_2–N–SO_2 framework of the anions as displayed in Fig. 2. The charge enclosed within these isosurfaces calculated from the HF wavefunction turns out to be 2.919 au for $NPSI^-$ and 3.211 au for $TFSI^-$ and accordingly the ratio of the charge to volume obtained therefrom is 0.038 for $NPSI^-$ and 0.029 for $TFSI^-$. Thus it may be inferred that the cation binding should be stronger in the case of $NPSI^-$. This may also partly be attributed to the stronger *–I* effect of the CF_3 groups of the TFSI anion. The self-consistent-field (SCF) electronic energies of LiNPSI, LiTFSI, and their corresponding anions are reported in Table 3. The complexation energies of the two anions were calculated by subtracting the sum of the electronic

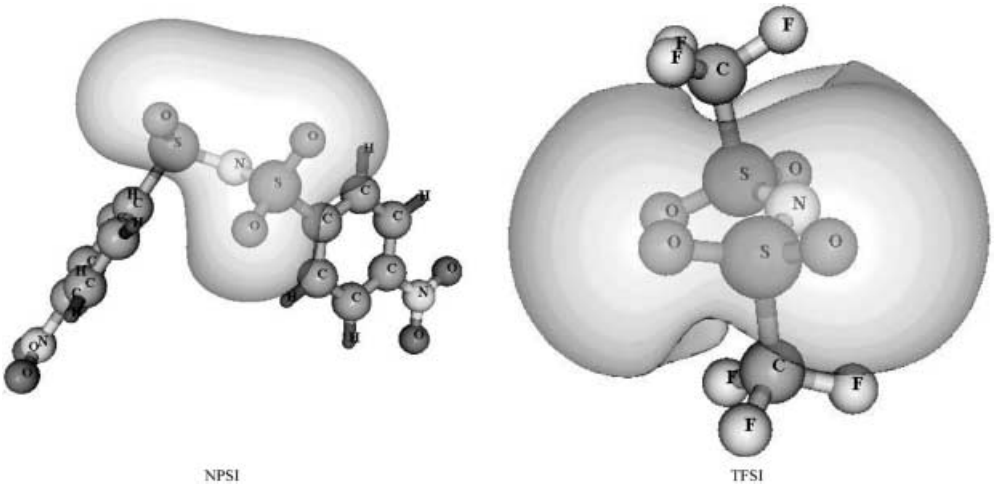

Fig. 2. Molecular electrostatic potential ($V = -370.2$ kJmol^{-1}) isosurfaces in the NPSI and bis(trifluromethanesulphone)imide (*TFSI*) anions

Table 3. Self-consistent field (*SCF*) energies of the anions and their Li^+ complexes. The SCF electronic energy for Li^+ is –7.235537 au. The zero-point-energy-corrected values are given in *parentheses*

	$NPSI^-$	Li^+NPSI^-	$TFSI^-$	Li^+TFSI^-
SCF energy (au)	−2016.035897 (−2015.806210)	−2023.507014 (−2023.274151)	−1821.187807 (−1821.126811)	−1828.654182 (−1828.590198)
Complexation energy (kJ mol^{-1})		−618.52 (−610.18)		−606.07 (−598.22)

energies of the individual free anion and of Li^+ from the total SCF electronic energy of the lowest-energy isomer of the complex. As shown in Table 3, the complexation energy for LiNPSI turns out to be 618.5 kJmol^{-1}, which is nearly 12.5 kJmol^{-1} higher than that of the LiTFSI complex. It may, therefore, be inferred that the complex formation seems to be more favored for the NPSI anion. The SPE exhibiting high ionic conductivity, which requires a high concentration of charge carriers, is facilitated by weakly coordinating anions such as LiTFSI. Thus, the observed lower ionic conductivities [16] of the SPE containing LiNPSI salts dissolved in PEO can be rationalized.

4 Conclusions

The present calculations predict two minimum-energy structures on the potential-energy surface for the LiNPSI complex compared to seven minima for LiTFSI owing to the less flexible S–N–S framework of the anion in the sufonylimide compared to $TFSI^-$. As noted for the LiTFSI complex [2], in the lowest-energy isomer of LiNPSI the anion also coordinates via two oxygens, one from each of the different SO_2 groups on the central nitrogen with the formation of a six-membered chelate. The relative stabilization energy of this isomer is predicted to be 55.9 kJmol^{-1} more than the other isomer where the bidentate coordination of the ligand takes place through nitrogen and oxygen atoms of the anion. These LiNPSI isomers can possibly be distinguished from the direction of frequency shift of the 1,239 and 1,205 cm^{-1} intense SO_2 stretching vibrations of the anion. The NO_2 groups substituted at both phenyl groups are expected to induce a stronger electron-withdrawing effect on the imide negative charge to provide large delocalization generating high charge carrier concentration. The present calculations, however, indicate that the NPSI anion binds more strongly to Li^+ than $TFSI^-$. This is evident from the charge density enclosed within the MESP isosurface encompassing the O_2S–N–SO_2 framework of the TFSI and NPSI anions. Thus, the formation of neutral ion pairs Li^+X^- (X = NPSI or TFSI) is favored in the case of the NPSI anion. This partly accounts for the observed lower conductivities of the sulfonyl imide containing SPE compared to the fluorinated imide dissolved in the same host polymer. In summary Li^+NPSI^- may not be as suitable as Li^+TFSI^- in PEO-based electrolytes.

Acknowledgement. S.P.G. acknowledges support from the Council of Scientific and Industrial Research [Project 01(1772)/02/EMR-II], New Delhi, India.

References

1. Gejji SP, Hermansson K, Tegenfeldt J, Lindgren J (1993) J Phys Chem 97: 11402
2. Gejji SP, Suresh CH, Babu K, Gadre SR (1999) J Phys Chem A 103: 7474
3. Rey L, Johansson P, Lindgren J, Lassegues JC, Grondin J, Servant L (1998) J Phys Chem A 102: 3249
4. Ratner MA, Shriver DF (1988) Chem Rev 88: 109
5. Addison CC, Amos DW, Sutton D (1968) J Phys Chem 88: 637

6. Burger K (1983) Studies in analytical chemistry 6: solvation and complex formation reaction in non-aqueous solvent. Elsevier, Amsterdam
7. Papke BL, Ratner MA, Shriver DF (1982) J Electrochem Soc 129: 1694
8. Armand MB, Chabagno JM, Duclot MJ (1979) In: Mundy JN, Shenoy GK (eds) Fast ion transport in solid electrodes and electrolytes. Elsevier North-Holland, Lake Geneva, Ill, pp
9. Gadre SR, Bhadane PK, Pundlik SS, Pingale SS (1996) In: Murray JS, Sen K (eds) Molecular electrostatics potentials: concepts and application. Elsevier, Amsterdam, p 219
10. (a) Legon AC, Millen DJ (1987) Chem Soc Rev 16: 467; (b) Dykstra CE (1989) J Am Chem Soc 111: 6168; (c) Alhambra C, Luque FJ, Orozco M (1995) J Phys Chem 99: 3084
11. Buckingham AD, Fowler PW (1983) J Chem Phys 79: 6426
12. Buckingham AD, Fowler PW (1985) Can J Chem 63: 2018
13. Politzer P, Truhlar DG (1981) Chemical applications of atomic and molecular electrostatics potentials. Plenum, New York
14. Bonaccorsi R, Scrocco E, Tomasi J (1970) J Chem Phys 52: 5270
15. Naray-Szabo G, Ferenczy GC (1995) Chem Rev 4: 829
16. Alloin F, Bayoud S, Azimipour B, Reibel L, Sanchez JY (2000) Electrochim Acta 45: 1193
17. Julien C, Nazri G (1994) Solid state batteries material design and optimization. Kluwer, Boston, Mass (1989) J Comput Chem 10: 209
18. Gejji SP, Suresh CH, Bartolotti LJ, Gadre SR (1997) J Phys Chem A 101: 5678
19. Frisch MJ, Trucks GW, Schlegel HB, Gill PMW, Johnson BG, Robb MA, Cheeseman JR, Keith T, Peterson GA, Montgomery JA, Raghavachari K, Al-laham MA, Zakrzewski VG, Oritz JV, Forseman JB, Cioslowski J, Stefanov BB, Nanayakkara A, Challacombe M, Peng CY, Ayala PY, Chen W, Wong MW, Andres JL, Replolge ES, Gomperts R, Martin RL, Fox DJ, Binkley JS, Defrees DJ, Baker J, Stewart JJP, Head-Gordon M, Gonzalez C, Pople JA (1995) GAUSSIAN94. Gaussian, Pittsburgh, Pa
20. (a) Limaye AC, Gadre SR (2001) Curr Sci India 80: 1298–1301; (b) Gadre SR, Shirsat RN (2000) Electrostatics of atoms and molecules. Universities Press, Hyderabad
21. Becke D (1993) J Chem Phys 98: 5684
22. Lee C, Yang W, Parr RG (1988) Phys Rev B 37: 785